Spacecraft Hazard Avoidance Utilizing Structured Light

Carl Christian Liebe, Curtis Padgett, Jacob Chapsky, Daniel Wilson, Kenneth Brown, Sergei Jerebets, Hannah Goldberg, Jeffrey Schroeder
Jet Propulsion Laboratory, California Institute of Technology
4800 Oak Grove Drive
Pasadena, CA 91109
818-354-7837
carl.c.liebe@jpl.nasa.gov

Abstract—At JPL, a <5 kg free-flying micro-inspector spacecraft is being designed for host-vehicle inspection. The spacecraft includes a hazard avoidance sensor to navigate relative to the vehicle being inspected. Structured light was selected for hazard avoidance because of its low mass and cost. Structured light is a method of remote sensing 3-dimensional structure of the proximity utilizing a laser, a grating, and a single regular APS camera. The laser beam is split into 400 different beams by a grating to form a regular spaced grid of laser beams that are projected into the field of view of an APS camera. The laser source and the APS camera are separated forming the base of a triangle. The distance to all beam intersections of the host are calculated based on triangulation.

TABLE OF CONTENTS

1. INTRODUCTION 1
2. MICRO-INSPECTOR MISSION AND SPACECRAFT DESCRIPTION 2
3. DESCRIPTION AND THEORY 3
4. SYSTEM …… 6
5. EXPERIMENTAL VALIDATION 7
6. SUMMARY 8
REFERENCES..... 8
ACKNOWLEDGEMENT…… 9
BIOGRAPHIES …… 9

1. INTRODUCTION

The primary range map sensors employed by NASA/DoD in past missions have been based on visible stereo cameras and laser radar [1]-[4]. Future missions have considered alternative technologies such as microwave radar [5] and structure from motion (single camera system), but all these systems are currently only in the developmental phase [6][7].

Radar has been used extensively on Earth for a variety of different applications. Radar sends out energy and is able to construct a range map of the surface. Its major drawbacks for space applications have been its cost, mass and power consumption. Laser radar has been utilized for rendezvous demonstration because of its lower mass, size and better resolution relative to microwave radar. However, this technology has still not been implemented on miniaturized spacecrafts.

For small Mars rovers, the technology of choice has been a stereo camera system. This approach determines range by matching tie points in one camera frame to the corresponding tie points in the opposite camera image. The difference in the angular position of the corresponding tie points in the two camera frames is related to range using triangulation [3]. The stereo system (as compared with radar) has excellent resolution at short ranges (range can be recovered for the great majority of shared pixels) and consumes only a few watts of power. With no active light source, a stereo system is limited to daytime operations (though a flash lamp could be added to provide a night capability).

A structured light system consists of an active light emitter that projects a pattern of light beams onto a surface in front of a camera that images the pattern [8]. The camera is offset from the light emitter. Each beam of light exits the light source grading at a fixed angle. Using that angle and the separation of the camera from the optics, range can be recovered from the image using triangulation. One way to generate a bundle of light beams is to pass a laser beam through a diffraction grating. This will split the original laser beam up into many individual laser beams that compose the pattern.

The different sensors that can be used to generate a range map are summarized in Table 1.

The mass requirement combined with the requirement to operate in a non sun illuminated environment, drove the decision to implement the hazard avoidance sensor utilizing structured light on the Micro-Inspector spacecraft being developed at JPL.

0-7803-9546-8/06/$20.00©2006 IEEE
IEEE AC paper #1071, Version 7, Updated Dec. 29 2005

Table 1. Different sensors for generating range maps

	Structured light system	Stereo Vision	Laser Radar	Microwave radar
Mass	<1 kg	<1 kg	6 kg	~30 kg
Power	A few watts	A few watts	<40 W	~200W
Max operating distance	Tens of meters	Tens of meters	2.5 km	Kilometer range
Night time operation	Yes	No	Yes	Yes
Computational Demand	< 10 MIPS	> 100 MIPS	< 1 MIPS	>> 100 MIPS

2. MICRO-INSPECTOR MISSION AND SPACECRAFT DESCRIPTION

The objective of the Micro-Inspector spacecraft [9] is to develop a small, low cost fully functional expendable spacecraft capable of external visual inspection of a host. A typical operational scenario of an inspection mission would be for the Micro-Inspector to launch attached to the host it plans to inspect. At some predetermined point in the host mission, it will release the Micro-Inspector with a simple command to a thermal separator. The thermal knife will cut through the wires holding the Micro-Inspector attached to its dock, gently releasing the inspector away from the host. The Micro-Inspector then initializes its bearings using a camera observing the celestial sphere and the hazard avoidance sensor. At this point the inspection of the host begins. The inspection profile will depend on the specific host, however the Micro-Inspector is capable of both circumnavigating the host for full inspection coverage, or station keeping to monitor a particular event or specific location. After the Micro-Inspector has completed its inspection, it will maneuver to a location to minimize the risk of impacting the host and causing potential damage.

Potential host missions and mission scenario include the Crew Exploration Vehicle, NASA's new replacement for the Space Shuttle. Inspection scenarios could include pre-inspection of a crewed lunar descent or Earth reentry spacecraft prior to descent maneuvers, or to provide monitoring of critical in-space assemblies or deployments. The Micro-Inspector's use of solar power and celestial navigation extend its operation beyond the limits of Earth orbit for use in missions to the Moon or Mars. Due to the small size and mass of the Micro-Inspector, multiple inspectors could be used on one host to monitor multiple locations simultaneously or to be used deployed at different times over the scope of the host mission.

The design is focused on safe operation to the host and its crew. This is done by maintaining a low mass inspector and limiting the potential damage even if the host is impacted. On board constraints and anomaly detection are driven by safe operation. In addition, the Micro-Inspector employs the laser based hazard avoidance sensor utilizing structured light to provide relative range measurements to the host.

The Micro-Inspector is designed to have a minimal effect upon its host by being small size and mass. Classified at the "nano" scale [10], the spacecraft is a rectangular box approximately 8" x 8" x 2" with a mass of just <5 kg. It is a fully functional autonomous spacecraft, made up of all subsystems of a typical spacecraft including power, thermal, command and data handing, telecommunications, propulsion, and attitude determination and control.

The spacecraft is composed of a sandwich structure consisting of the propellant tank, multilayer circuit board, and payload components. All subsystem electronics are integrated onto one circuit board reducing the need for cables and harnesses. On top of the tank and circuit board is the solar panel assembly, a mushroom cap top mounted on fiberglass standoffs which thermally isolate the panel from the main structure. The solar array is housed on the top of the solar panel assembly, providing the main source of power to the spacecraft electronics.

Contained under the solar panel assembly, a number of payload components are mounted on standoffs over the circuit board including the battery assemblies, pressure sensors, gyroscope, sun sensor, multiple cameras, and laser with grating. The heart of the Micro-Inspector avionics is a Virtex II Pro FPGA with two embedded PowerPC processors. These processors run the commands and sequences to control the Micro-Inspector to provide inspection services and monitor internal health sensors to determine spacecraft health. All communications with the Micro-Inspector are performed with the host using short range UHF transceivers. There is no capability for communication directly to the Earth. Command and command sequences are sent from the host to the inspector with images of the host and spacecraft health data transmitted to the host. Eight small thrusters located along the perimeter of the spacecraft enable a full 6 DOF motion relative to the host.

Celestial navigation is used to determine spacecraft attitude in order to extend operation beyond the constraints of Earth orbit. Attitude sensors include a MEMS gyroscope, a micro sun sensor [11], and cameras used as star trackers. The Micro-Inspector contains six cameras which are used as star trackers, visual inspection of the host, and detector for the laser based hazard avoidance sensor. A sketch of the micro-inspector spacecraft is shown in Figure 1.

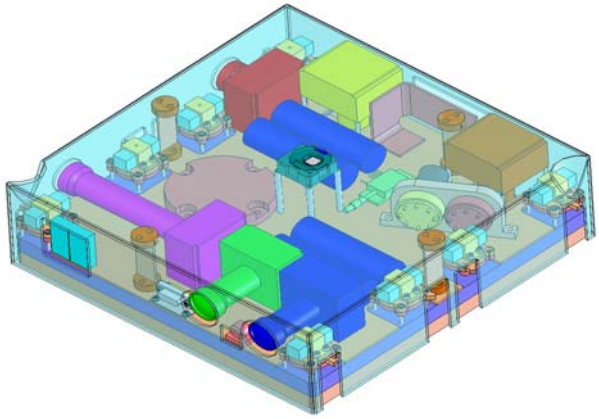

Figure 1 - Sketch of the Micro-Inspector spacecraft

3. DESCRIPTION AND THEORY

The hazard avoidance sensor is based on the same principles as stereovision – it determines the distance to the laser spots utilizing triangulation. In stereovision, two cameras are located some distance apart and observe the same point simultaneously. The same image feature is found and correlated in the two images, and the 3D position is found by triangulation [12]. One of the difficulties in stereovision is to figure out which image features in the first image correspond to which image features in the second image (tie points). This is in particular a problem when observing a homogeneous featureless surface on a spacecraft. Also, stereovision will not operate in darkness without active illumination.

Assuming that the camera and laser/grating system is aligned perfectly (i.e. the x axis of the focal plane is parallel with the baseline), then the y component of the spot is observed at the same y value on the camera for all distances. This is true for a co-boresighted stereo camera system as well – a feature found in the left image will appear at the same y value in the right image. The distance from the camera to the target surface will determine the horizontal displacement of the feature in the images.

The idealized scenario for a single laser beam triangulation is shown in Figure 3. In this scenario a coordinate system is defined with the origin at the exit aperture of the laser. The x-axis of the coordinate system is oriented towards the equivalent pinhole of the camera. The laser and the equivalent pinhole are separated by a baseline, B. The distance from the laser to the target is Z. It is observed in Figure 3 that the distance to the target can be determined from the equation:

$$\frac{B}{Z} = \tan\alpha \Leftrightarrow Z = B\cot(\alpha) \qquad (1)$$

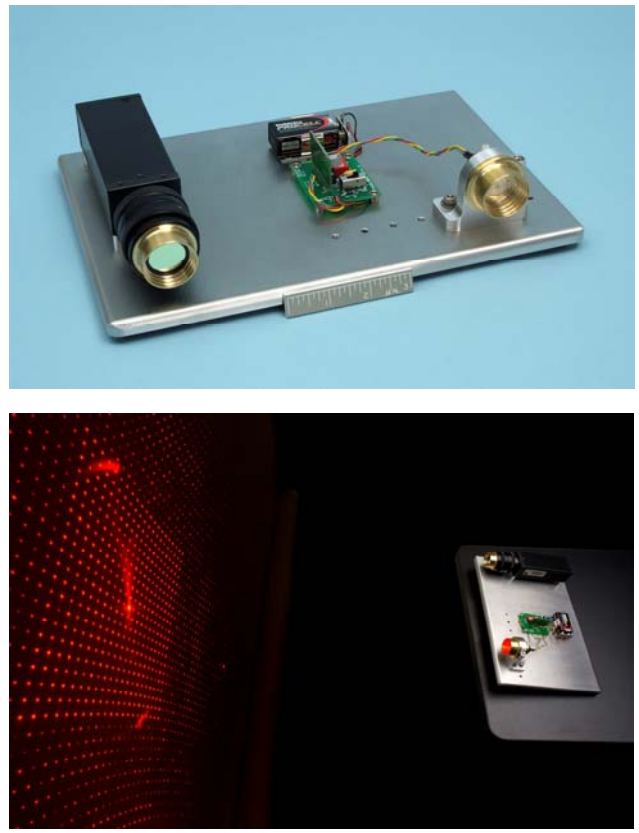

Figure 2 – Top: Image of the hazard avoidance sensor breadboard. The commercial camera is shown with a bandpass filter mounted on the lens. In the center of the plate is the laser drive electronics and to the right of the photograph is the laser diode, collimating lens and the diffraction grating. Bottom: Breadboard illuminating flat surface in front of the breadboard.

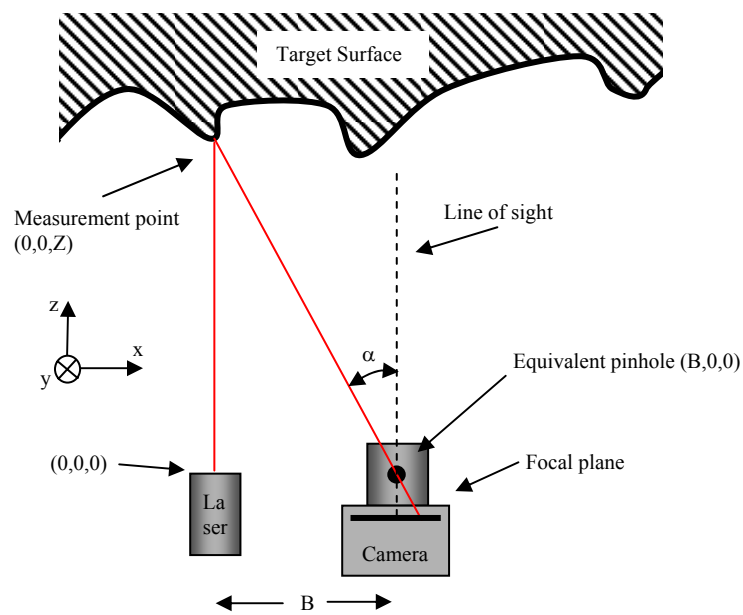

Figure 3 - Sketch of an idealized system for laser triangulation

The discussion up to this point has assumed an idealized system. However, the components of the system will be misaligned. The way that we have defined the coordinate system (the x-axis starting at the laser exit aperture and going towards the equivalent pinhole of the lens) prohibits unwanted translations in the system. All errors show up as rotational errors. A non-idealized system is sketched in Figure 4.

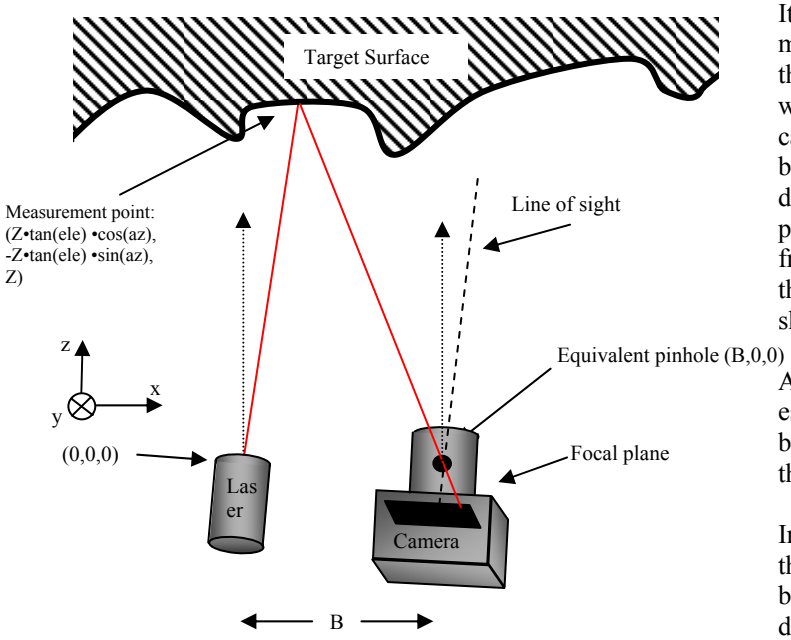

Figure 4 - Sketch of the non-idealized system

In Figure 4, it is observed that there are 6 parameters that describe the geometry: 1) The baseline separation between laser and camera (B). 2) The elevation (El) and azimuth (Az) angle that the laser beam is offset relative to pointing along the z axis and 3) a rotation matrix A (3 degrees of freedom) that describes the rotation of the camera relative to the ideal situation. This is a total of 6 degrees of freedom. Also, internal parameters of the camera (e.g. effective focal length and optical distortion) are additional degrees of freedom. For a conventional calibration, taking a large number of measurements and solving an over-determined set of equations would derive the unknown constants.

An alternative to the conventional calibration method is to employ an empirical method to calibrate the system. The reason for choosing an empirical calibration is that it requires less effort to implement.

A setup is made where the non-idealized system is placed in front of a flat wall at a minimum distance (e.g. 1 meter). An image is acquired and the centroid of the spot is calculated. The system is then moved to a new distance (e.g. 1 meter and 10 centimeters) and a new image is acquired and the centroid is calculated. This procedure is repeated up to the maximum distance that the system is required to work. The scenario is shown in Figure 5**.**

The measured centroids during the calibration sequence are superimposed on an artificial image as shown in Figure 6.

After the calibration, the system is pointed at a surface of unknown distance and an image is acquired and the centroid is calculated. An example centroid of unknown distance is shown in red in Figure 7.

It is observed that the measured centroid lies between 1.4 meters and 1.5 meters. The unknown distance is therefore in that range. A more accurate estimate is made the following way: A straight line is projected through all of the calibration points in an RSS sense. This is shown as the black dotted line in Figure 7. The red dot is then projected down onto the dotted line. Now all calibration points are plotted in a new coordinate system. The distance (in pixels) from the first calibration point is the unit on the x-axis and the distance to the target is the unit on the y-axis. This is shown in Figure 8.

A polynomial is fitted though the points and it is possible to estimate the Z distance based on the projection onto the line between the calibration points. In the example from before, the red dot is estimated to be at a distance of 1.44 meters.

In the discussions up to this point, we have discussed the theory for a single spot. However, suppose that two laser beams illuminated the scene. It would then be possible to determine the 3D position of the two spots independently utilizing the same theory on each spot. We can continue to add spots as long as we can uniquely associate each spot with its individual calibration curve.

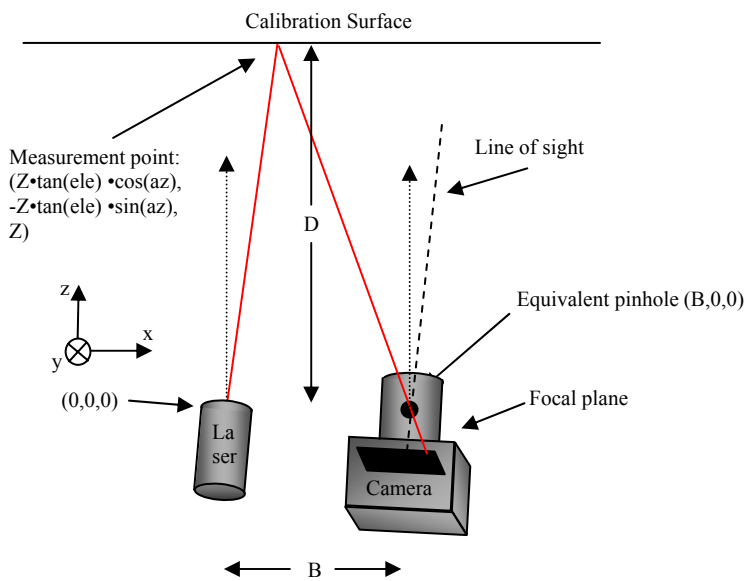

Figure 5 - The calibration setup

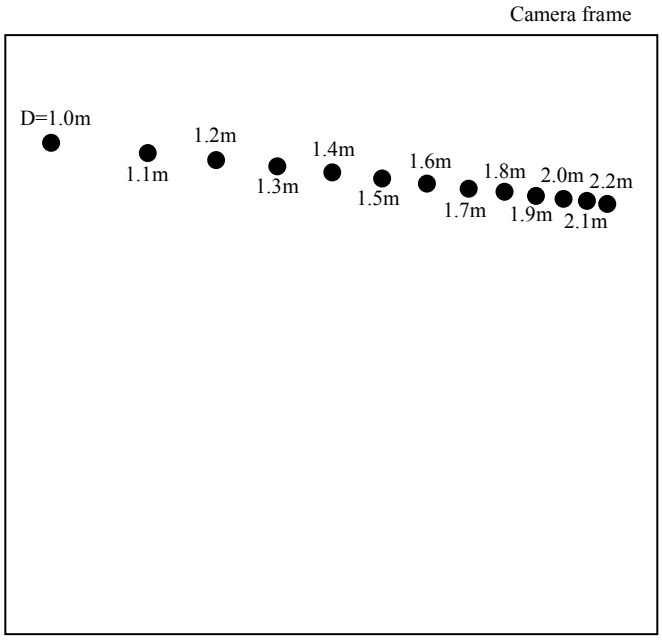

Figure 6 - An example of a set of centroids from the series of calibration images

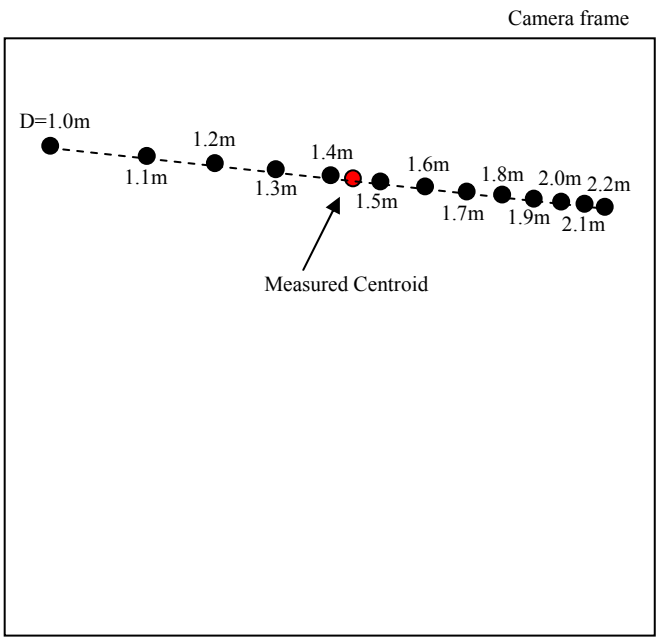

Figure 7 - Measurement of an unknown distance (red dot) utilizing a calibration curve

It is impractical to add hundreds of individual lasers to illuminate the scene in front of the camera. Therefore, the laser beam is passed through a diffraction grating. The interference pattern induced by the grating can split the outgoing laser beam into *m* **x** *n* beams. Each beam exits the optic at a fixed angle (α, γ) from the incident beam. The number and angle of a spot is determined by the properties of the grating and the laser wavelength.

If a row of spots all fall on the same image row, different Z distances will tend to displace the image locations (x's) closer together, possibly interfering with each other. It is also possible that some portions of the surface might shadow the camera from imaging some of the spots (spot dropout). In either case, the problem of identifying the spot and its associated angle is made difficult without taking some precautions to guard against aliasing or dropout.

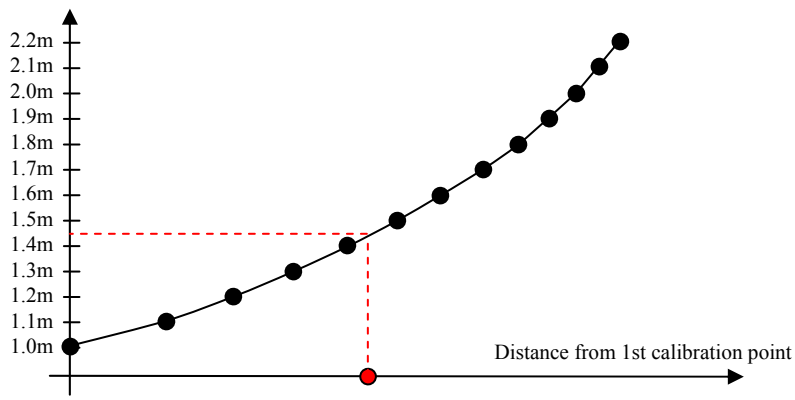

Figure 8 - The calibration curve. The red line represents the centroid from the unknown distance

The approach we've taken to uniquely identify each spot involves rotating the grid produced by the laser/grating system by an angle *r* around the direction of the laser beam. Also, the baseline, B and the geometry of the setup is constrained to limit the amount of dispersion (=movement on the focal plane), d, experienced by a spot over the operating ranges of the system. To insure that neighboring spots do not overlap, *r* and B are selected to provide each spot a unique area on the image plane. The area needs to be of sufficient width to provide reasonable range resolution and of sufficient height to insure that neighboring spots do not overlap. This is sketched in Figure 9.

Ideally, the rotation should be sufficient to insure that the divergence of a spot *d* should not interfere with its neighbors that have a separation of *s* (also in pixels).

$$r = \arcsin(s/d) \qquad (2)$$

In the example in Figure 9 the grid is rotated so that the next spot in the grid is 4 scan lines displaced. With a rotation, spots on other rows in the grid are rotated onto a given spot's scan line. Even though off-row spots are separated further in angular space, spot disparity could still lead to spot aliasing. To eliminate this possibility, the horizontal angular separation between spots can be increased, or the baseline between the camera and the laser/grating can be shortened. Given a maximum allowed divergence d (in angle), and a minimum range (Z_{min}), the maximum baseline can be approximated to be:

$$B = Z_{min} * \tan(d) \qquad (3)$$

Decreasing the dynamic range or increasing the grid spacing provides additional flexibility in designing the structured light system.

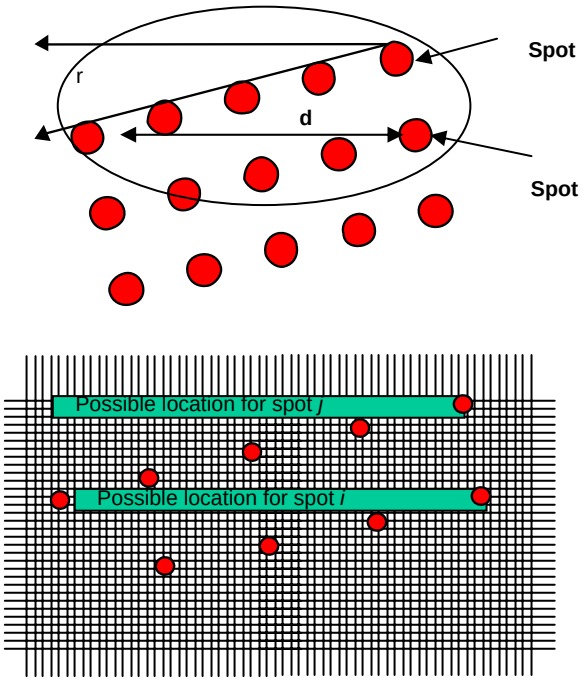

Figure 9 - The upper sketch shows the grid rotated by an angle *r* while the lower sketch depicts the motion induced on a spot by allowed ranges.

For baselines less than B in Equation 3, a spot is constrained to move in an area that is unique to the point. Spots found in the area bounded by their maximum divergence and their location at Z_{min} will have valid ranges. Aliasing is not a problem as each spot's area is unique and spot loss simply means that the range map has one less entry.

4. SYSTEM

A block diagram of the hazard avoidance sensor is shown in Figure 10.

For the hazard avoidance sensor, the 808 nm Coherent F6-808-2.5-2400-200-FC laser was selected as the laser source. This laser was selected because it is powerful (2.4W), detectable by a visible APS camera and it had previously been space qualified. The most difficult issue for the hazard avoidance sensor is to operate in bright sun illumination, because the laser spots illuminating the host spacecraft must have brightness comparable to the sun illumination to be reliable detected and centroided. The narrow band pass filter of the system is another way to increase the signal relative to the sun. However, 10 nm is the narrowest that can be used because the perceived wavelength of the laser light changes with the incident angle (up to 12.5 degrees).

The beam splitting diffractive optical element (DOE) was designed to produce a square array of 21 x 21 spots with a full divergence angle of 26.2° along the horizontal and

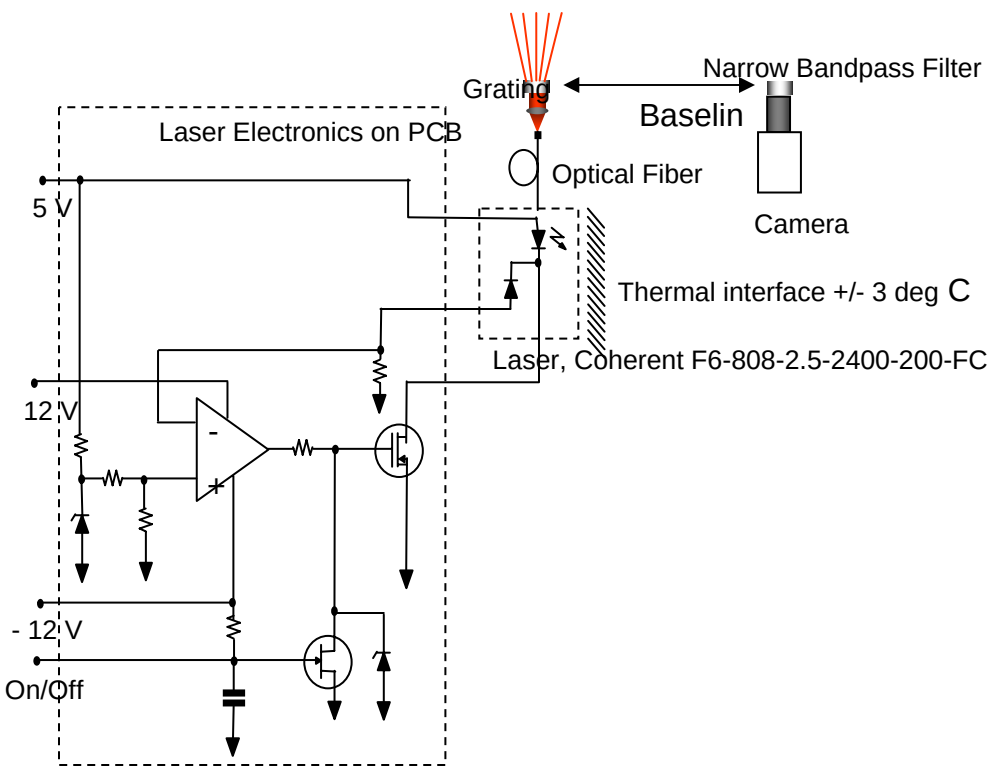

Figure 10 - Block diagram for hazard avoidance sensor

vertical axes. The DOE is actually a two-dimensional computer-generated hologram (CGH) grating with a period of 28 µm (square unit cell). This period produces the desired spot array divergence at the laser wavelength of 635 nm. The CGH unit cell is composed of 28 x 28 square pixels 1 µm in size, the depths of which were designed using an iterative Fourier transform algorithm [13] to diffract light uniformly into the 21 x 21 array of spots. Each pixel imposes a phase delay on the light passing through it, so that in the far field, interference produces the desired spot pattern. The DOE was fabricated in polymethylmethacrylate (PMMA) on fused silica by direct-write electron beam lithography in JPL's Micro Devices Laboratory [14].

5. EXPERIMENTAL VALIDATION

An experiment was conducted with the bread board to determine the maximum operating range in a sun illuminated environment. The breadboard was taken outside and a picture was acquired. The image is shown in Figure 11. Within a fraction of a second the laser is turned off and another image is acquired. The two images are subtracted. The difference image is shown in Figure 12 (in false colors). The identified centroids are shown in Figure 13.

Figure 11 - Image of laser illumined surface in sun illuminated environment. The distance to the bucket was 50 inches and it was illuminated with the 20 mW breadboard system shown in Figure 2.

In Figure 13, it is observed that approximately half of the laser spots are identified (the regular pattern on the bucket) and a number of spurious centroids are also identified. The spurious spots do not matter because they do not appear in locations where laser spots can appear and therefore they are ignored. The image was acquired at a distance of 48 inches from the bucket with the breadboard system shown in Figure 2. However, only ~50% of the laser spots are identified. The spot intensity variations are 25%. Therefore, if the laser intensity was raised 50%, the vast majority of the spots would be detected. Or, in other words, the laser intensity is only 67**%** of what it should be to detect all spots. This experiment was conducted at 12/31/2005, 15:00 in Pasadena, California. The sun was at 22° elevation, 2.7 airmasses and was attenuated to 37% relative to its intensity outside the atmosphere [15]. In other words, the laser would be (relative to the sun) **0.37** times dimmer outside the earth atmosphere. The experiment is conducted with the breadboard 632 nm laser. In the real experiment the laser will be at 808 nm. The sun intensity going from 632 nm to 808 nm is only 71% or in other words the intensity ratio is going to be **1.41** higher. The laser used in the experiment was due to eye safety adjusted to 20 mW output., The real laser for the hazard avoidance will be adjusted to 2.4W. Therefore the real system will be **120 times** brighter. It is also assumed that in a flight system the number of spots will be decreased from 400 to 200. This will increase the spot intensity a factor of **2**. Based on this discussion it is possible to calculate how bright the flight system would be under space conditions relative to the experiment: 0.67 * 0.37 * 1.41 * 120 * 2 = 83.9 times. The detection range is proportional to the square root of the distance, so the flight system will operate sqrt(83.9)=9.2 times further away than the 50 inch or a distance of ~12 meters.

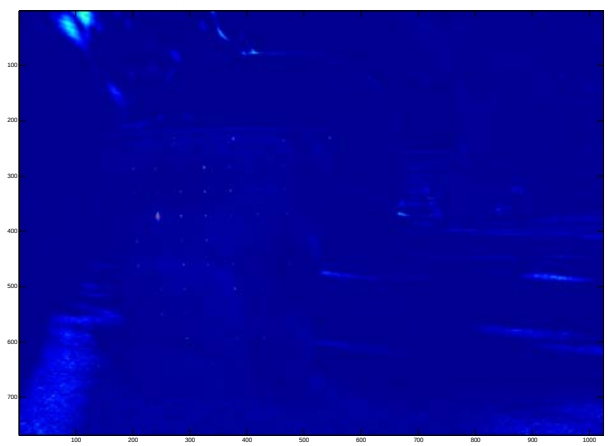

Figure 12. Difference image of Figure 11 with and without laser illumination

Another experiment was conducted (not related to the scenario shown in Figure 11) to establish the accuracy of the hazard avoidance sensor. In this experiment, the hazard avoidance sensor taken to a distance of 2 meters to a wall and an image was acquired. Simultaneously a total station (an instrument used by surveyors to measure accurate angles and distances) was used to measure the distance between the wall and the breadboard. The distance to the wall was then increased slightly and a new measurement was taken out to a distance of 12 meters. The measured distance (Z) with the total station is shown as a function of the x-coordinate of a single specific spot's centroid in Figure 14. The X-coordinate is plotted because the displacement primarily shows up in this coordinate.

A fifth order polynomial is fitted to the data and the residual is plotted as function of distance. This plot is shown in Figure 15. It is observed in Figure 15 that the RMS error for

the system is 4 cm. The baseline between the laser and the camera was 20 cm.

Figure 13 - Identified centroids in Figure 12

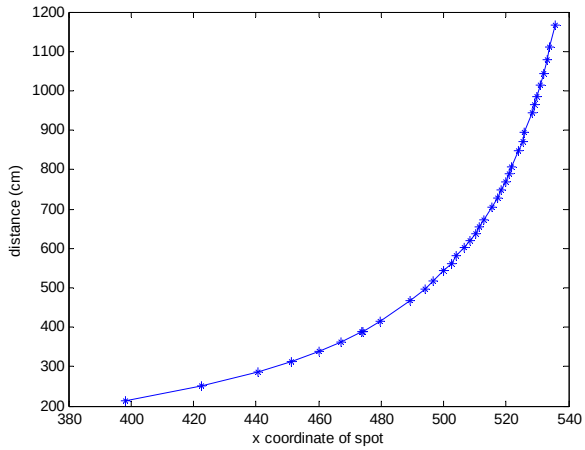

Figure 14 - The distance to the target (Z) plotted as a function of the x coordinate of a single individual spot

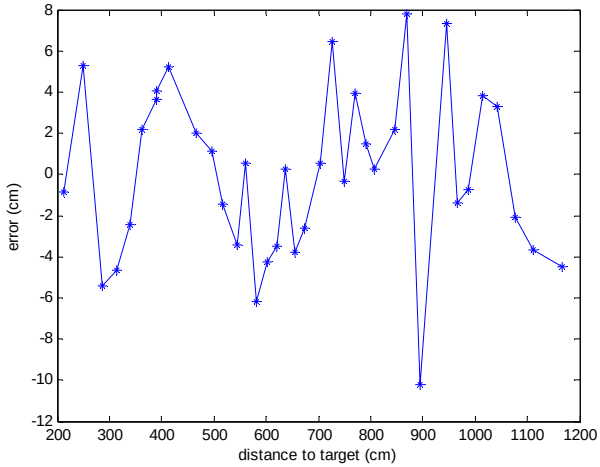

Figure 15 – The measured distance uncertainty for the hazard avoidance system

6. SUMMARY

A hazard avoidance sensor is being developed at the Jet Propulsion Laboratory, California Institute of Technology. The hazard avoidance sensor is based on structured light, because of its low mass, night time operation, maturity and low cost. The sensor operates by emitting 400 laser beams towards the target being inspected. A camera separated by a baseline distance is imaging the laser spots and calculating the distance to all laser spots based on triangulation. This paper described the principle of operation of the system. A laboratory breadboard model has been built utilizing a commercial camera and an eye safe laser. Images of real scenarios are presented. It is shown that the system will be able to operate at distances up to 12 meters and the accuracy of the system is 4 cm. The hazard avoidance sensor will be utilized on a <5 kg Micro-Inspector spacecraft.

REFERENCES

[1] C.C.Liebe, A.Abramovici, R.Bartman, R.Bunker, J.Chapsky, C.Chu, D.Clouse, J.Dillon, B.Hausmann, H.Hemmati, R.Kornfeld, C.Kwa, S.Mobasser, M.Newell, C.Padgett, W.T.Roberts, G.Spiers, Z.Warfield, M.Wright: Laser Radar for Spacecraft Guidance Applications, In proceedings of the 2003 IEEE Aerospace conference, Montana, Volume: 6 , March 8-15, 2003, Pages:6_2647 - 6_2662.

[2] R.Kornfeld, R.Bunker, G.Cucullu, J.Essmiller, F.Y.Hadaegh, C.C.Liebe, C.Padgett, E.Wong: New Millennium ST6 Autonomous Rendezvous Experiment (ARX), in the proceedings of the 2003 IEEE Aerospace conference, Montana, March 2003, Volume: 1 , 8-15 March 2003.

[3] A.Eisenman, C.C.Liebe, M.W. Maimone, M.A.Schwochert, and R.G. Willson: Mars Exploration Rover Engineering Cameras, Proceedings of the SPIE #4540: Sensors, Systems, and Next Generation Satellites V, Toulouse France, September 2001.

[4] http://www.vs.afrl.af.mil/News/05-23.swf, cited 12/1/2005

[5] Brian D. Pollard, Gregory Sadowy, Delwyn Moller, and Ernesto Rodríguez: A Millimeter-Wave Phased Array Radar for Hazard Detection and Avoidance on Planetary Landers, In proceedings of the 2003 IEEE Aerospace conference, Montana, March 2003, in print.

[6] A. Johnson, Y. Cheng, L. Matthies: Machine Vision for Autonomous Small Body Navigation, 2000 IEEE Aerospace conference, March 2000.

[7] Carl Christian Liebe, Curtis Padgett, Johnny Chang, Three Dimensional Imaging Utilizing Structured Light, In proceedings of the 2004 IEEE Aerospace conference, Montana, March 2004, in print.

[8] Matthies, L. and Balch, T. and Wilcox, B. Fast Optical Hazard Detection for Planetary Rover Using Multiple Spot Laser Triangulation. ICRA 1997.

[9] J. Mueller, L. Alkalai, C. Lewis: Micro-Inspector Spacecraft for Space Exploration Missions, 2005 Space Technology and Applications International Forum, Albuquerque, NM, February 2005.

[10] (Spacecraft classification: http://centaur.sstl.co.uk/SSHP/sshp_classify.html)
[11] S.Mobasser, C.C.Liebe: MEMS based sun sensor on a chip, Presented at the 2003 IEEE Conference on Control Applications, 2003. CCA 2003. Proceedings of 2003 IEEE Conference, Volume: 1, 23-25 June 2003. Pages: 1483 - 1487 vol.2.
[12] Rafael C. Gonzalez, Richard E. Woods: Digital Image Processing, Addison-Wesley Pub Co; 2nd edition (January 15, 2002) ISBN: 0201180758.
[13] R. W. Gerchberg and W. O. Saxton, "A practical algorithm for the determination of the phase from image and diffraction plane pictures," Optik 35, 237–246 (1972).
[14] D. W. Wilson, R. E. Muller, P. M. Echternach, and J. P. Backlund, "Electron-beam lithography for micro- and nano-optical applications," in Micromachining Technology for Micro-Optics and Nano-Optics III, edited by Eric G. Johnson, Gregory P. Nordin, Thomas J. Suleski, Proceedings of SPIE Vol. 5720 (SPIE, Bellingham, WA, 2005), pp. 68-77.
[15] National Renewable Energy Laboratory, Department of Energy: http://www.nrel.gov/midc/solpos/solpos.html, cited 12/29/2005

ACKNOWLEDGEMENT

The research described in this paper was carried out at the Jet Propulsion Laboratory, California Institute of Technology and was sponsored by the National Aeronautics and Space Administration. References herein to any specific commercial product, process or service by trademark, manufacturer, or otherwise, does not constitute or imply its endorsement by the United States Government or the Jet Propulsion Laboratory, California Institute of Technology.

BIOGRAPHIES

Dr. Carl Christian Liebe received the M.S.E.E. degree in 1991 and the Ph.D. degree in 1994 from the Department of Electro physics, Technical University of Denmark. Since 1997, he has been an employee at the Jet Propulsion Laboratory, California Institute of Technology. Currently, he is a senior member of the technical staff in the Laser Remote Sensing Group in the In Situ Instrument Systems Section. His research interests include new technologies and applications for avionics sensors and metrology systems.

Dr. Curtis Padgett received his Ph.D. from the Computer Science and Engineering Department at the University of California at San Diego (UCSD) in 1998. He received his M.S. degree from the same department in 1992. He has been employed at the Jet Propulsion Laboratory, California Institute of Technology, Pasadena since 1993. He is a Senior Member of the Technical Staff in the Machine Vision group of the Mobility Section where he works on remote sensing applications for space systems. His research interests include algorithm optimization, machine vision, and artificial intelligence applied in classification and pattern recognition tasks.

Jacob Chapsky is a senior electronics design engineer with 46 years of experience in designing military, space and industrial subsystems. He has an M.S.E.E. degree from USC. He was a chief scientist at Hughes Aircraft where he was responsible for many space-deployed subsystems. As a principal engineer at California Institute of Technology he played a critical part with his designs in achieving the $2{\cdot}10^{-9}$ m/√Hz noise floor for the Gravitational Wave detector. He was also a program engineer for 2 Apollo instruments deployed on the Moon in 1969.

Dr. Daniel W. Wilson received the Ph.D. in Electrical Engineering from Georgia Institute of Technology in 1994. His thesis research included investigations electron waveguiding in semiconductor nanostructures and optical waveguiding in photorefractive crystals. Following graduation, he worked as a Postdoctoral Fellow at Georgia Tech on rigorous modeling of optical propagation in waveguides and non-periodic diffractive structures. In October 1994, he joined the Microdevices Laboratory at JPL where he has focused on the design, modeling, and electron-beam fabrication of diffractive optical components and novel optical instruments. He has been a key contributor to the successful development of convex diffraction gratings, transient-event imaging spectrometers, and particle velocity sensors. In 2003, he won JPL's Lew Allen Award for Excellence for his work on electron-beam fabricated convex gratings.

Kenneth Brown received his B.S. in Computer Science and Physics from Morehouse College in Atlanta, and a M.S. in Applied Physics from Clark Atlanta University. As an electro-optical system engineer, Brown is currently a System Engineering Analyst for the Space Interferometry Mission (SIM) External Metrology. SIM will determine the positions and distances of stars several hundred times more accurately than any previous program. Ken Brown developed the bread board system.

Dr. Sergei Jerebets received the M.S. Physics degree in 1997 from Washington State University (WA) and Ph.D. Physics in 2002 from Wesleyan University (CT). Sergei Jerebets has been with Jet Propulsion Laboratory, California Institute of Technology since then: first as a Caltech postdoctoral scholar and recently as a member of the technical staff in the Precision Motion Control & Celestial Sensors Group. His current interests include ACS Sensors development, image acquisition and analysis.

Hannah Goldberg, received her M.S.E.E and B.S.E from the Department of Electrical Engineering and Computer Science at the University of Michigan in 2004 and 2003 respectively. She has been employed at the Jet Propulsion Laboratory, California Institute of Technology since 2004 as a member of the technical staff in the Precision Motion Control and Celestial Sensors group. Her research interests include the development of nano-class spacecraft and microsystems.

Jeff Schroeder is a Senior Technical Assistant who has worked at JPL for 26 years. He specializes in mechanical design and fabrication, and has worked on many flight and development projects. His interest in astronomy includes 25 years as a planetarium lecturer, construction of an 11" refracting telescope, and eclipse chasing around the world. The recently upgraded 48" Palomar Schmidt telescope uses a CCD camera that he designed and built for the Near Earth Asteroid Tracking (NEAT) program. For this and earlier work on the program, asteroid 19290 Schroeder was named this year. Presently, in his spare time, he is working on his second homebuilt airplane.